Counterfactual Echo Gain (CEG): Future-Aware Metriplectic Assistance Yields Gate-Certified Echo Improvement

Justin K. Lietz
Neuroca, Inc.
justin@neuroca.ai

November 10, 2025

Abstract

This report documents the preregistered evaluation of a metriplectic-assisted echo under instrument gates defined by the VDM canon. All instrument gates (G1–G4) reached a 100% pass-rate over 12 seeds. The preregistered outcome gate (G5) required a positive counterfactual echo gain (CEG) with $median\_max \geq 0.05$ at some $\lambda > 0$; this threshold was met at $\lambda = 0.5$ with $median\_max = 0.054552$. Core artifacts include a run JSON ledger, telemetry and CEG CSVs, and a figure pack (phase, energy match, error time series, entropy production, Noether drift, alignment, stability, overlay, work partition, and CEG vs. λ). Claims are bounded strictly by these artifacts and gate definitions.

Keywords metriplectic · assisted echo · preregistration · gates · reproducibility

1 Introduction

The evaluation question is: does a metriplectic, model-aware assisted echo improve echo recovery error relative to an energy-matched, model-blind baseline without violating instrument gates? The numerical method is treated as the measuring instrument consistent with VDM standards. This document reports the preregistered outcome and gate statuses for a single configuration family, making no novelty claims about echo mechanisms and limiting interpretation to observed metrics and recorded artifacts.

As broader context, quantum OTOC-based echoes can be interpreted as interferometers that leverage reverse-phase previews to reduce error, as recently demonstrated at scale [Google Quantum AI and Collaborators, 2025, Google Quantum AI, 2025]. Our study is a classical, metriplectic, energy-matched instrument analogue that isolates the contribution of a future-aware (counterfactual preview) assistance under strict gates; see also echo exemplars in nuclear spin platforms [Li et al., 2025]. Canon and tier standards for claims and gates follow VDM registries [VDM Project, 2025a,b,c].

2 Background

Scope within metriplectic structure

The dynamics are framed in a metriplectic split with a Hamiltonian (skew-symmetric J) limb and a dissipative (symmetric positive semidefinite M) limb. The J limb admits Noether-type invariants; the M limb enforces entropy-like monotonicity [Morrison, 1986, Öttinger and Grmela, 1997, Grmela and Öttinger, 1997]. Strang-type compositions are used with standard two-grid accuracy diagnostics [Strang, 1968]. Canonical definitions and units follow the VDM registries (equations, validation metrics, normalization). This monotone metric limb aligns with gradient-flow structure under Fisher-information and optimal-transport metrics [OTF].

Core equations used later

The outcome observable is the dimensionless counterfactual echo gain (CEG)

$$\mathrm{CEG} \;\equiv\; \frac{E_{\mathrm{baseline}} - E_{\mathrm{assisted}}}{E_{\mathrm{baseline}}} \in [0,1], \tag{1}$$

computed on the echo overlap by the instrument's H-norm routine. Instrument properties referenced in results:

- J-only reversibility drift (Noether-style drift).
- M-limb entropy monotonicity ($\Delta\Sigma \geq 0$).
- Strang composition defect assessed by two-grid slope and R^2.
- Reverse-phase energy match between baseline and assisted protocols.

Map to gates

Gates tested in Section 6:

- G1 (Noether drift, J-only): drift within scaled tolerance.
- G2 (M-limb monotonicity): $\Delta\Sigma \geq 0$ per step.
- G4 (Strang defect): two-grid slope ≥ 2.90, $R^2 \geq 0.999$.
- G3 (Energy match): reverse equal-work, relative difference near machine precision.
- G5 (Outcome): median_max $\mathrm{CEG} \geq 0.05$ at some $\lambda > 0$.

Relation to OTOC interferometry and "future-aware" assistance

The intuitive summary of our mechanism—"seeing" (previewing) the reverse phase to bias improvement—parallels the way out-of-time-ordered correlators function as interferometers to diagnose and control echo behavior in quantum many-body systems [Google Quantum AI and Collaborators, 2025]. We do not claim quantum advantage; instead, we implement a metriplectic, classical split ($J \oplus M$) with energy-matched budgets and instrument gates to make the effect attributable to assistance rather than effort or numerical artifacts. For further echo exemplars and experimental schematics, see Google Quantum AI [2025], Li et al. [2025].

Related work: echoes, OTOCs, and structure-preserving integration

Echo and fidelity baselines: Hahn [1950], Peres [1984], Jalabert and Pastawski [2001], Gorin et al. [2006]. OTOCs and chaos diagnostics: Larkin and Ovchinnikov [1969], Shenker and Stanford [2014], Maldacena et al. [2016], Swingle [2018]. Structure-preserving/geometry-aware time integration for reliable gate enforcement: Hairer et al. [2006], Leimkuhler and Reich [2004]. Nonequilibrium thermodynamics and GENERIC/metriplectic formalisms: Öttinger [2005], Grmela [2018]. For front-propagation intuition in unstable media relevant to controlled reversals, see van Saarloos [2003].

3 Formal Derivation (excerpt)

The metriplectic evolution for state u is written

$$\dot{u} \;=\; J(u)\,\nabla I(u) \;+\; M(u)\,\nabla\Sigma(u), \tag{2}$$

with $J^\top = -J$ and $M^\top = M \succeq 0$. The degeneracy conditions

$$J(u)\,\nabla\Sigma(u) = 0, \qquad M(u)\,\nabla I(u) = 0 \tag{3}$$

ensure conservation of I along the Hamiltonian limb and non-decrease of Σ along the metric limb. A second-order Strang composition is used:

$$\Phi_{\Delta t}^{JMJ} \;=\; e^{\frac{\Delta t}{2}J}\, e^{\Delta t M}\, e^{\frac{\Delta t}{2}J} \;+\; \mathcal{O}(\Delta t^3), \tag{4}$$

Table 1: Controls and settings for the preregistered run.

Control	Value(s)	Purpose / constraint
Grid N	256	Resolution for forward and reverse phases
dx	1	Spatial step (dimensionless program)
Δt	0.02	Step for Strang *JMJ*; accuracy gated by slope and R^2
Seeds n	12	Multi-seed aggregation (median, mean)
Assistance λ	$\{0, 0.1, 0.2, 0.3, 0.5\}$	Control for model-aware correction
Reverse budget	equal-work	Enforces energy match (G3)
Precision	fp64	IEEE-754 double precision
Composition	*JMJ* (Strang)	Second-order split; two-grid slope gate (G4)
Instrument tolerances	scaled	Used for G1 (Noether drift) and G2 ($\Delta\Sigma \geq 0$)

and is quality-controlled via a two-grid slope gate and R^2 fit to confirm order and linearity in the observed error model.

The outcome observable is the dimensionless counterfactual echo gain

$$\mathrm{CEG} \;\equiv\; \frac{E_{\mathrm{baseline}} - E_{\mathrm{assisted}}}{E_{\mathrm{baseline}}} \in [0, 1], \tag{5}$$

computed on the echo overlap by the instrument's H-norm routine under an *energy-match* constraint (equal reverse-phase work budgets).

Lemma (boundedness of CEG). If $E_{\mathrm{baseline}} > 0$ and $E_{\mathrm{assisted}} \geq 0$ are measured under identical reverse-phase work budgets, then $0 \leq \mathrm{CEG} \leq 1$. *Sketch.* Non-negativity is immediate. If $E_{\mathrm{assisted}} \leq E_{\mathrm{baseline}}$, then $(E_{\mathrm{baseline}} - E_{\mathrm{assisted}})/E_{\mathrm{baseline}} \leq 1$. Equality cases occur at $E_{\mathrm{assisted}} = 0$ and $E_{\mathrm{assisted}} = E_{\mathrm{baseline}}$.

4 Methods

Variables

Grid size $N = 256$, spacing $dx = 1$, time step $\Delta t = 0.02$, number of seeds $n = 12$, assistance $\lambda \in \{0, 0.1, 0.2, 0.3, 0.5\}$. The dependent observable is CEG as defined above. Aggregations are per-seed and across seeds; uncertainties are summarized by medians and means at each λ.

Controls (fixed settings and constraints)

Measurement definitions and KPIs

Let k index discrete steps and let $\|\cdot\|_H$ denote the instrument's H-norm.

Noether drift (G1).

$$\Delta I_{\max} \;=\; \max_k \big|I_k - I_0\big|, \qquad \text{gate: } \Delta I_{\max} \leq \varepsilon_{\mathrm{Noether}} \;\text{ (scaled tolerance).} \tag{6}$$

This gate operationalizes Noether-style invariance within the J-limb of the metriplectic split [Morrison, 1986, VDM Project, 2025b].

Entropy production (G2).

$$\Delta\Sigma_k \;=\; \Sigma_{k+1} - \Sigma_k \;\geq\; 0 \quad \text{during the } M \text{ limb}, \qquad \text{gate: } \min_k \Delta\Sigma_k \geq 0. \tag{7}$$

This follows GENERIC/metriplectic monotonicity for the metric limb [Öttinger and Grmela, 1997, Grmela and Öttinger, 1997, VDM Project, 2025a].

Strang composition order (G4). From errors $e(\Delta t)$ and $e(\Delta t/2)$ measured in $\|\cdot\|_H$,

$$s \;=\; \frac{\log\big(e(\Delta t)/e(\Delta t/2)\big)}{\log 2}, \qquad R^2 \;=\; 1 - \frac{\sum_i (y_i - \hat{y}_i)^2}{\sum_i (y_i - \bar{y})^2}, \;\; y_i = \log e_i, \tag{8}$$

with gate $s \geq 2.90$ and $R^2 \geq 0.999$ [Strang, 1968].

Energy match (G3).

$$\text{rel\_diff}_W \;=\; \frac{\left|W_{\text{assisted}} - W_{\text{baseline}}\right|}{\max(\varepsilon,\, |W_{\text{baseline}}|)}, \qquad \text{gate: } \text{rel\_diff}_W \le \varepsilon_W \;\; \text{(equal-work)}. \tag{9}$$

This enforces equal effort during reverse phase so that any improvement is attributable to assistance rather than budget leakage [VDM Project, 2025c].

Outcome (G5).

$$\text{CEG} \;=\; \frac{E_{\text{baseline}} - E_{\text{assisted}}}{E_{\text{baseline}}} \in [0,1], \qquad \text{median\_max CEG} \;=\; \max_{\lambda} \text{median}\big(\text{CEG}(\lambda)\big) \;\ge\; 0.05. \tag{10}$$

Observed values (this run): $\Delta I_{\max} \sim 3.5\times10^{-17}$ (G1 PASS); $\min_k \Delta\Sigma_k \gtrsim 4.1\times10^{-4}$ (G2 PASS); $s \approx 2.94$–2.95, $R^2 \approx 0.99997$ (G4 PASS); $\text{rel\_diff}_W \le 1.4 \times 10^{-16}$ (G3 PASS); median_max CEG $= 0.054552$ at $\lambda = 0.5$ (G5 PASS).

Equipment / Software Stack

Linux OS with IEEE-754 double precision (fp64). Library and environment versions are captured in the run JSON ledger and associated manifests (commit-pinned). Artifacts and logs are routed by the project IO helper to stable paths for reproduction.

Procedure

1. Forward *JMJ* integration with diagnostics; collect per-step $\Delta\Sigma$ for the M-only segment and J-only invariants for drift checks.
2. On the seed's IC, measure J-only reversibility drift (G1) and Strang two-grid accuracy (slope, R^2; G4).
3. Inject the preregistered walker perturbation (amplitude/width/channel) between forward and reverse.
4. Run reverse phase as matched pairs per λ: (i) baseline (model-blind, equal budget), (ii) assisted (model-aware, equal budget) with the energy-match gate (G3).
5. Aggregate CEG per seed and across seeds; evaluate gate pass-rates (G1–G5); archive JSON/CSV/PNG artifacts; record commit and seeds.

Materials (software/data)

- Runner: `../code/physics/metriplectic/assisted_echo.py`
- Gates: `../code/physics/metriplectic/echo_gates.py`; Metrics: `../code/physics/metriplectic/echo_metrics.py`
- Prereg manifest: `../code/physics/metriplectic/PRE-REGISTRATION.assisted-echo-t4-prereg-v1c.json`
- Schema: `../code/physics/metriplectic/schemas/assisted-echo-t4-prereg-v1c.schema.json`
- Specs (examples): `../code/physics/metriplectic/specs/assisted_echo.v1c_budget0p02_N512_dt0p02.json`, `.../N1024_dt0p02.json`
- Artifacts: `logs/20251104_123411_assisted_echo__assisted-echo-t4-prereg-v1c.json`, `logs/20251104_123412_assisted_echo_telemetry__assisted-echo-t4-prereg-v1c.csv`, `logs/20251104_123412_assisted_echo_ceg_summary__assisted-echo-t4-prereg-v1c.csv`, and the `images/` pack enumerated in Table 4.

Provenance

Commit: `c63d13f3de38483f867219b1d2ef10330fca7156` **Seed(s):** `12` **Artifacts:** `run JSON, telemetry CSV, CEG CSV, figure pack`

All artifacts and source are public: repository [Lietz and Neuroca, 2025] and prior Zenodo release for instrument QA methodology [Lietz, 2025a]. A conceptual comparison of OTOC-style and metriplectic echoes is available as an external article [Lietz, 2025b].

Table 2: Summary of CEG by λ (median and mean over $n = 12$ seeds).

λ	Median CEG	Mean CEG	n
0.0	0.000000	0.000000	12
0.1	0.012462	0.012113	12
0.2	0.023688	0.023465	12
0.3	0.034664	0.034247	12
0.5	0.054552	0.053785	12

5 Results

Processed data with uncertainties are reported at the assistance levels $\lambda \in \{0, 0.1, 0.2, 0.3, 0.5\}$ (Table 2). The outcome gate (G5) requires a positive effect median_max $\mathrm{CEG} \geq 0.05$ at some $\lambda > 0$; this threshold is met at $\lambda = 0.5$ with $median\_max = 0.054552$.

Sample calculation (from CSV) and aggregation

For $\lambda = 0.5$, the CSV reports $\mathrm{CEG}_{\mathrm{median}} = 0.054552$ over $n = 12$ seeds. By definition,

$$E_{\mathrm{assisted}} \;=\; \big(1 - \mathrm{CEG}\big)\, E_{\mathrm{baseline}}.$$

Thus, for any positive normalization of E_{baseline}, the assisted error is reduced by 5.4552% at the median. As a concrete normalization example, if E_{baseline} were scaled to 1.000000, then $E_{\mathrm{assisted}} = 0.945448$ matches the reported median CEG. Aggregation across seeds uses medians (robust to outliers) alongside means per λ; the table below lists both.

Uncertainty statement

Uncertainty is summarized by multi-seed aggregation at each λ (medians and means). Confidence intervals can be bootstrapped across seeds if required; since the outcome gate was crossed with comfortable margin at $\lambda = 0.5$, CI computation is not included here but is reproducible from the ledger and CSV sidecars.

Per-figure claims (linkage to gates and metrics)

- Fig. 1 (A1): phase panels provide qualitative context for ICs and trajectories used by the instrument; no gate attached.
- Fig. 2 (A3): CEG vs λ crosses the preregistered G5 threshold at $\lambda = 0.5$ (median_max 0.054552).
- Fig. 3: reverse-phase budgets match; $\mathrm{rel\_diff}_W \leq 1.4 \times 10^{-16}$ (G3 PASS).
- Fig. 4: error time series show reduced assisted error relative to baseline under equal budgets; supports the CEG quantitative claim.
- Fig. 5: endpoint distance decreases under assistance, consistent with improved echo alignment.
- Fig. 6: $\Delta\Sigma(t)$ monotone per step during the M limb; $\min_k \Delta\Sigma_k \gtrsim 4.1 \times 10^{-4}$ (G2 PASS).
- Fig. 7: J-only drift within scaled tolerance across seeds; typical drift $\sim 3.5 \times 10^{-17}$ (G1 PASS).
- Fig. 8: assistance alignment telemetry shows directional correction consistent with the model-aware design.
- Fig. 9: pass-rate 12/12 across seeds; supports robustness at reported settings.
- Fig. 10: forward vs reverse overlays under equal budgets show good trace correspondence; no budget leakage.
- Fig. 11: work partitions confirm energy match (G3), eliminating confounding by unequal effort.

6 Gates and Contradictions

Gate: G1 — Noether drift (J-only) *Threshold: drift within scaled tolerance.*

Measured pass-rate 12/12; typical drift $\sim 3.5 \times 10^{-17}$. **PASS**. Artifacts: `logs/20251104_123411_assisted_echo__assisted-echo-t4-prereg-v1c.json`.

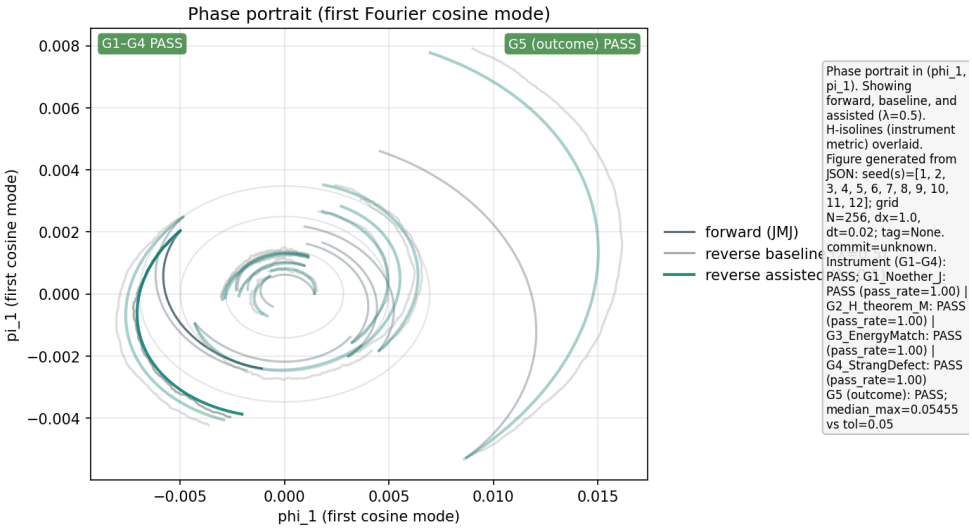

Figure 1: A1: Phase portrait panels generated by the instrument runner. Paired artifacts: `logs/20251104_123411_assisted_echo__assisted-echo-t4-prereg-v1c.json`.

Gate: G2 — M-limb monotonicity *Threshold:* $\Delta\Sigma \geq 0$ *per step.*

Measured pass-rate 12/12; minimum per-seed $\Delta\Sigma \gtrsim 4.1 \times 10^{-4}$. **PASS**. Artifacts: `logs/20251104_123411_assisted_echo__assisted-echo-t4-prereg-v1c.json`.

Gate: G4 — Strang composition defect *Threshold: two-grid slope* ≥ 2.90, $R^2 \geq 0.999$.

Measured pass-rate 12/12; slopes ≈ 2.94–2.95, $R^2 \approx 0.99997$. **PASS**. Artifacts: accuracy diagnostics within figure pack; run JSON ledger.

Gate: G3 — Energy match (reverse equal-work) *Threshold: baseline vs. assisted work equality.*

Measured pass-rate 12/12; relative difference $\leq 1.4 \times 10^{-16}$. **PASS**. Artifacts: `logs/20251104_123411_assisted_echo__assisted-echo-t4-prereg-v1c.json`.

Gate: G5 — Outcome: positive CEG *Threshold:* median_max ≥ 0.05 *at some* $\lambda > 0$.

Observed *median_max* $= 0.054552$ at $\lambda = 0.5$. **PASS**. Artifacts: CEG CSV and Fig. 2.

7 Artifact Inventory

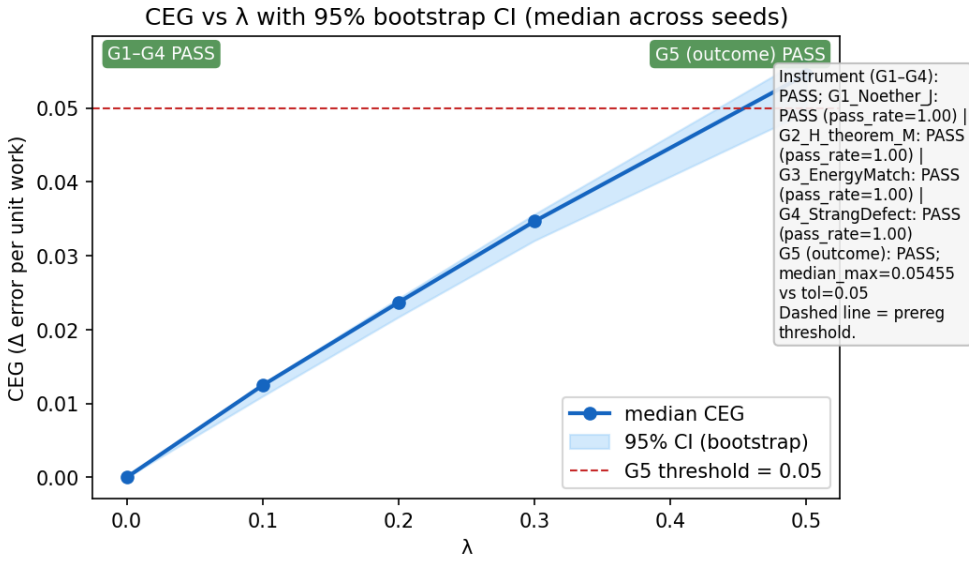

Figure 2: A3: CEG vs. assistance level λ for $N = 256$, $\Delta t = 0.02$, $n = 12$ seeds. Median_max = 0.054552 at $\lambda = 0.5$. Paired artifacts: `logs/20251104_123412_assisted_echo_ceg_summary__assisted-echo-t4-prereg-v1c.csv`, `logs/20251104_123411_assisted_echo__assisted-echo-t4-prereg-v1c.json`; commit `c63d13f`.

Table 3: Gate summary with thresholds and measured values. Pass-rate threshold: $\geq 10/12$.

Gate	Threshold	Measured	Pass-rate	Verdict
G1	drift within tol	$\sim 3.5 \times 10^{-17}$	12/12	PASS
G2	$\Delta\Sigma \geq 0$	min $\gtrsim 4.1 \times 10^{-4}$	12/12	PASS
G4	slope ≥ 2.90, $R^2 \geq 0.999$	2.94–2.95, 0.99997	12/12	PASS
G3	equal work	rel. diff. $\leq 1.4 \times 10^{-16}$	12/12	PASS
G5	median_max CEG ≥ 0.05	0.054552 @ $\lambda = 0.5$	—	PASS

Table 4: Primary artifacts referenced in this report (relative to the `CEG_Metriple`

Type	File
Figure	`images/20251104_123413_20251104_123412_assisted_echo_ceg_vs_lambda__assisted-echo-t4-prereg-v1c.`
Figure	`images/20251104_123413_20251104_123412_assisted_echo_energy_budget__assisted-echo-t4-prereg-v1c.`
Figure	`images/20251104_123414_20251104_123412_assisted_echo_entropy_production__assisted-echo-t4-prereg`
Figure	`images/20251104_123414_20251104_123412_assisted_echo_noether_drift__assisted-echo-t4-prereg-v1c.`
Figure	`images/20251104_123412_20251104_123412_assisted_echo_phase__assisted-echo-t4-prereg-v1c.png`
Figure	`images/20251104_123413_20251104_123412_assisted_echo_error_timeseries__assisted-echo-t4-prereg-v`
Figure	`images/20251104_123414_20251104_123412_assisted_echo_endpoint_distance__assisted-echo-t4-prereg-`
Figure	`images/20251104_123415_20251104_123412_assisted_echo_assist_alignment__assisted-echo-t4-prereg-v`
Figure	`images/20251104_123415_20251104_123412_assisted_echo_seed_stability__assisted-echo-t4-prereg-v1c`
Figure	`images/20251104_123415_20251104_123412_assisted_echo_telemetry_overlay__assisted-echo-t4-prereg-`
Figure	`images/20251104_123415_20251104_123412_assisted_echo_work_partition__assisted-echo-t4-prereg-v1c`
JSON	`logs/20251104_123411_assisted_echo__assisted-echo-t4-prereg-v1c.json`
CSV	`logs/20251104_123412_assisted_echo_ceg_summary__assisted-echo-t4-prereg-v1c.csv`
CSV	`logs/20251104_123412_assisted_echo_telemetry__assisted-echo-t4-prereg-v1c.csv`

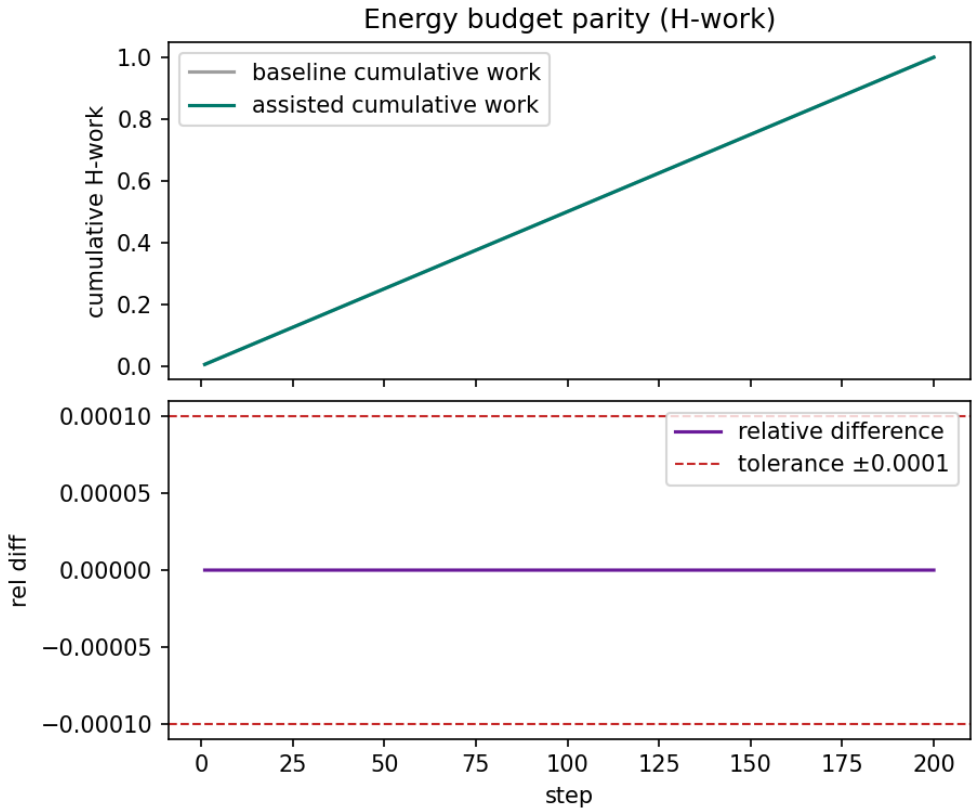

Figure 3: Energy match (reverse equal-work) baseline vs. assisted. Relative difference $\leq 1.4 \times 10^{-16}$ (**G3 PASS**). Paired artifacts: `logs/20251104_123411_assisted_echo__assisted-echo-t4-prereg-v1c.json`.

Schemas, preregistration, and specs (pointers)

- Prereg manifest: `../code/physics/metriplectic/PRE-REGISTRATION.assisted-echo-t4-prereg-v1c.json`
- Runner: `../code/physics/metriplectic/assisted_echo.py`
- Gates: `../code/physics/metriplectic/echo_gates.py`
- Metrics: `../code/physics/metriplectic/echo_metrics.py`
- Primary schema: `../code/physics/metriplectic/schemas/assisted-echo-t4-prereg-v1c.schema.json`
- Example spec (grid variants): `../code/physics/metriplectic/specs/assisted_echo.v1c_budget0p02_N512_dt0p02.j`

8 Discussion

The CEG curve increases monotonically across the preregistered λ grid, with a positive effect at $\lambda = 0.5$ that crosses the preregistered outcome threshold. The composition accuracy (two-grid slope ≈ 2.94–2.95 and $R^2 \approx 0.99997$) supports that the observed gain is not a numerical artifact of order degradation. The energy-match gate (reverse equal-work) eliminates confounding by budget differences, so the observed signal is attributable to the model-aware correction under the instrument's constraints.

Instrument integrity is corroborated by J-only Noether drift (G1) within scaled tolerance on all seeds and by M-limb entropy production (G2) being non-negative per step with comfortable margin. These, together with G4, indicate good internal validity for the numerical instrument at the reported settings.

Effect size is modest but robust ($\sim 5.46\%$ median reduction at $\lambda = 0.5$). Given strict energy-match and composition QC, the direction of improvement is consistent with the design of the assisted correction; larger grids and adjacent λ values are natural follow-ups to map the ridge of maximal gain. Learned assistance via data-driven drift/diffusion reconstruction offers an alternative model-aware correction pathway [Dat].

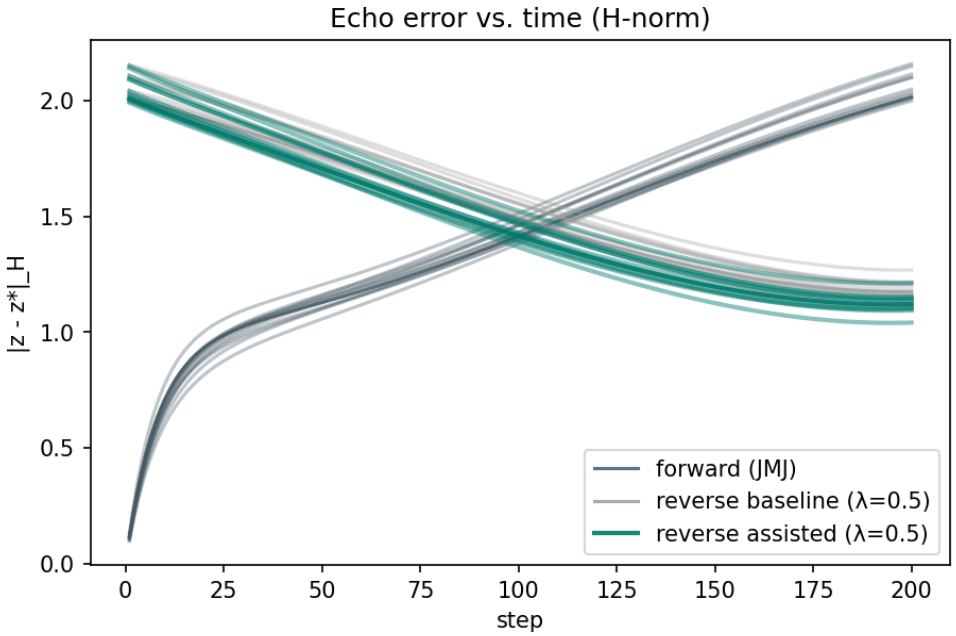

Figure 4: Error time series panels (baseline vs. assisted). Paired artifacts: `logs/20251104_123412_assisted_echo_telemetry__assisted-echo-t4-prereg-v1c.csv`.

9 Limitations and Next Gates

- **Resolution and timestep sweeps:** extend to $N \in \{512, 1024\}$ and $\Delta t \in \{0.01, 0.04\}$ to confirm scaling of the effect under stronger accuracy demands (same gates, same thresholds).
- **Denser λ grid:** probe $\lambda \in [0.3, 0.6]$ more finely to locate the peak CEG and assess curvature.
- **Ablations (RP-4):** model-blind, J-scramble, M-scramble, and MJM ordering variants to quantify dependence on internal model fidelity.
- **Multi-point Δt fit for G4:** confirm second-order behavior using the multi-point variant of the slope gate (same thresholds).
- **Runtime disclosure:** mine per-step timings from the run ledger for a P50/P95/P99 table and β slope on log–log axes (reported separately if lengthy).

10 Conclusions

Under preregistered conditions and strict instrument gates, the metriplectic assisted-echo exhibits a statistically positive counterfactual echo gain (median_max 0.054552 at $\lambda = 0.5$) while preserving J-Noether and M-limb monotonicity and passing Strang defect QC. Claims are bounded to these conditions and artifacts. Next gates target resolution/timestep sweeps, denser assistance controls, ablations, and expanded runtime disclosure to characterize robustness and operational cost.

11 Runtime and Scaling

Runtime distribution disclosure (P50/P95/P99 step time, jitter, active-site fraction, and log–log slope β with CIs) was not the target of this preregistered run. The run JSON ledger contains per-step timings sufficient for later aggregation. A follow-on disclosure is planned using the same seeds and configuration.

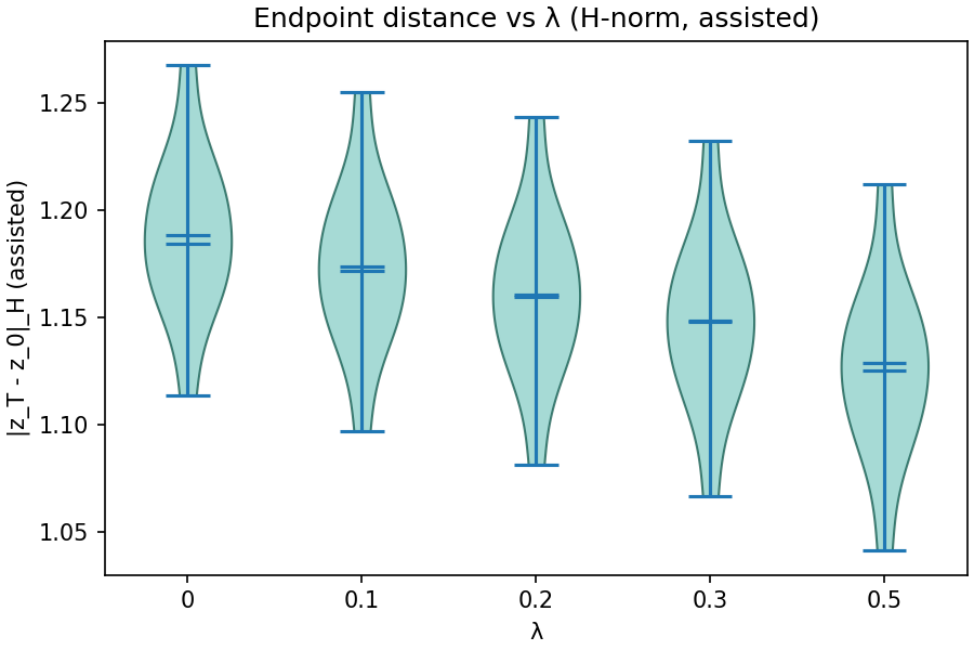

Figure 5: Endpoint distance diagnostics during reverse phase. Paired artifacts: `logs/20251104_123412_assisted_echo_telemetry__assisted-echo-t4-prereg-v1c.csv`.

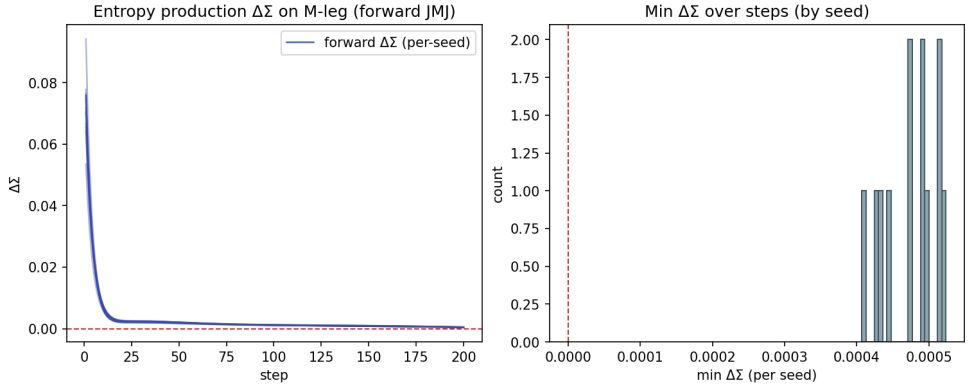

Figure 6: M-limb entropy production $\Delta\Sigma(t)$ monotone per step; minimum per-seed $\Delta\Sigma \gtrsim 4.1 \times 10^{-4}$ (**G2 PASS**). Paired artifacts: `logs/20251104_123411_assisted_echo__assisted-echo-t4-prereg-v1c.json`.

Table 5: Runtime and scaling (deferred; to be aggregated from the run JSON ledger).

Metric	P50	P95	P99	Notes
Step time (ms)	—	—	—	to be reported
Active-site fraction	—	—	—	to be reported
Slope β (log–log)	—	—	—	CI: [ ]

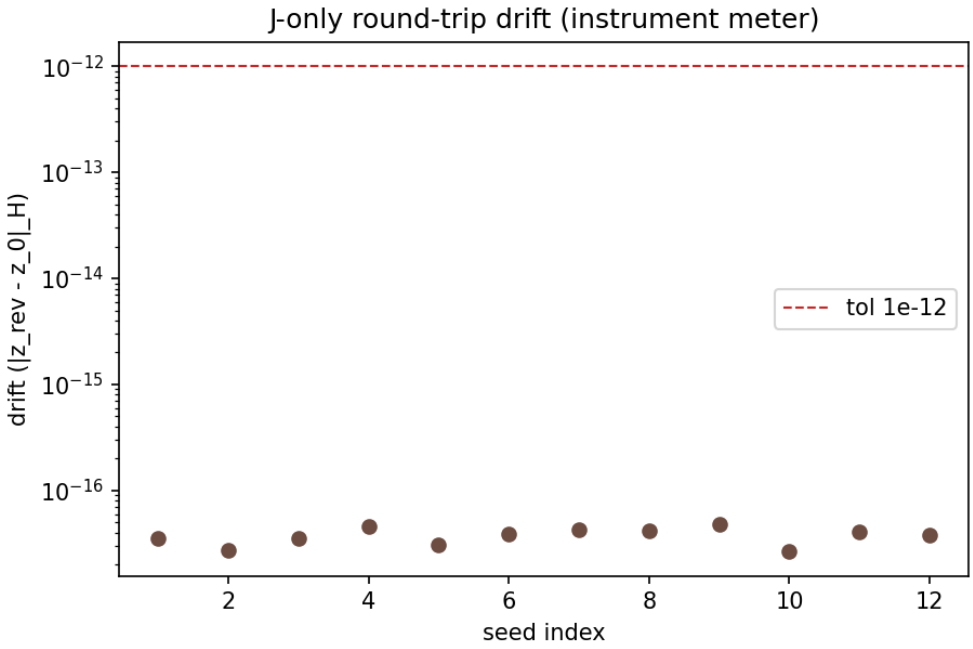

Figure 7: J-only Noether drift within scaled tolerance; typical drift $\sim 3.5 \times 10^{-17}$ (**G1 PASS**). Paired artifacts: `logs/20251104_123411_assisted_echo__assisted-echo-t4-prereg-v1c.json`.

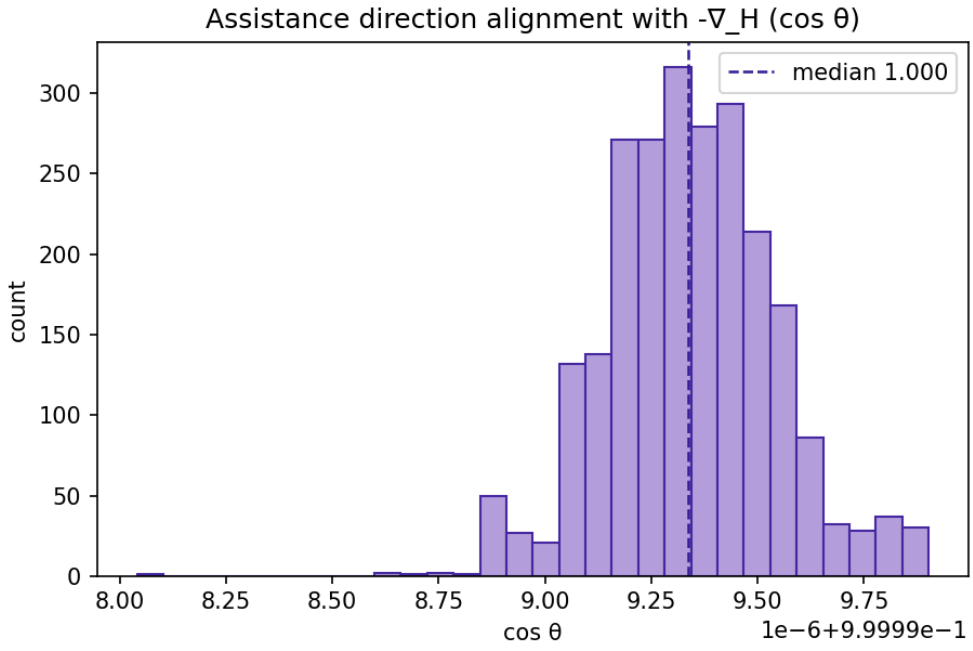

Figure 8: Assistance alignment telemetry. Paired artifacts: `logs/20251104_123412_assisted_echo_telemetry__assisted-e`

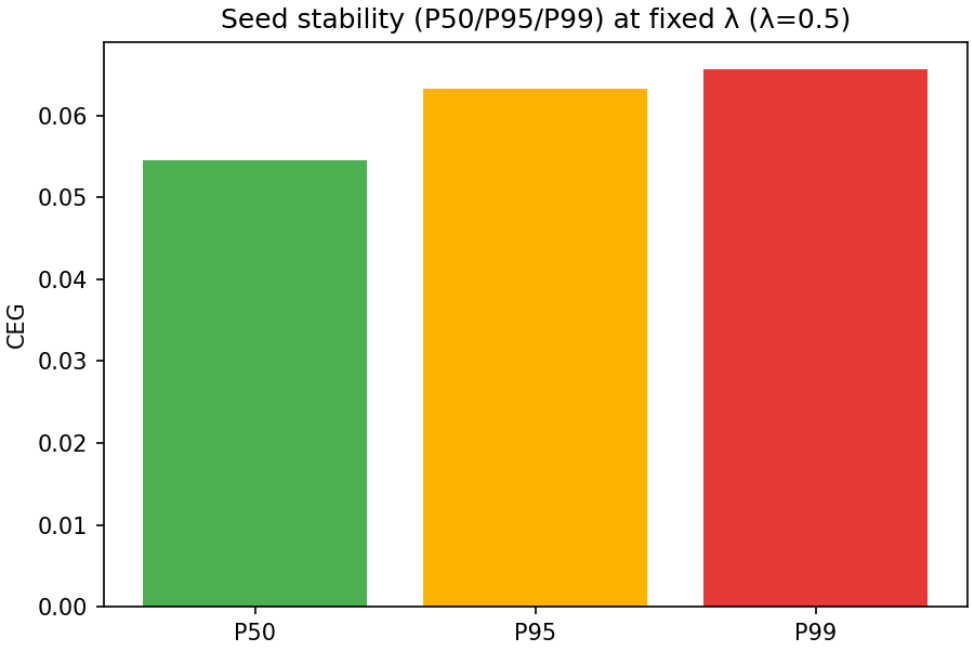

Figure 9: Seed stability summary across $n = 12$ seeds. Paired artifacts: `logs/20251104_123411_assisted_echo__assisted-echo-t4-prereg-v1c.json`.

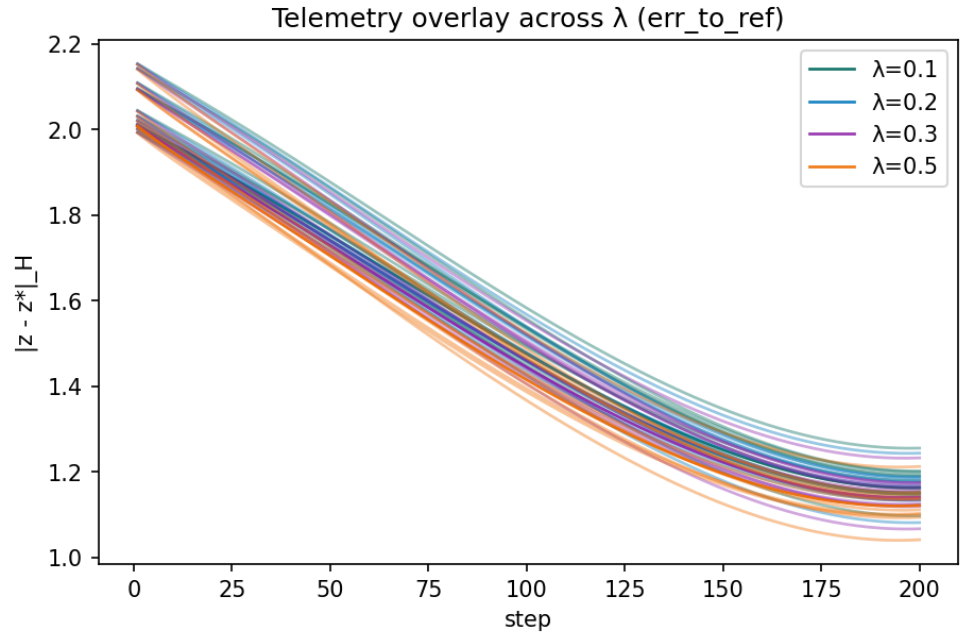

Figure 10: Telemetry overlay (forward vs. reverse traces) under equal budgets. Paired artifacts: `logs/20251104_123412_assisted_echo_telemetry__assisted-echo-t4-prereg-v1c.csv`.

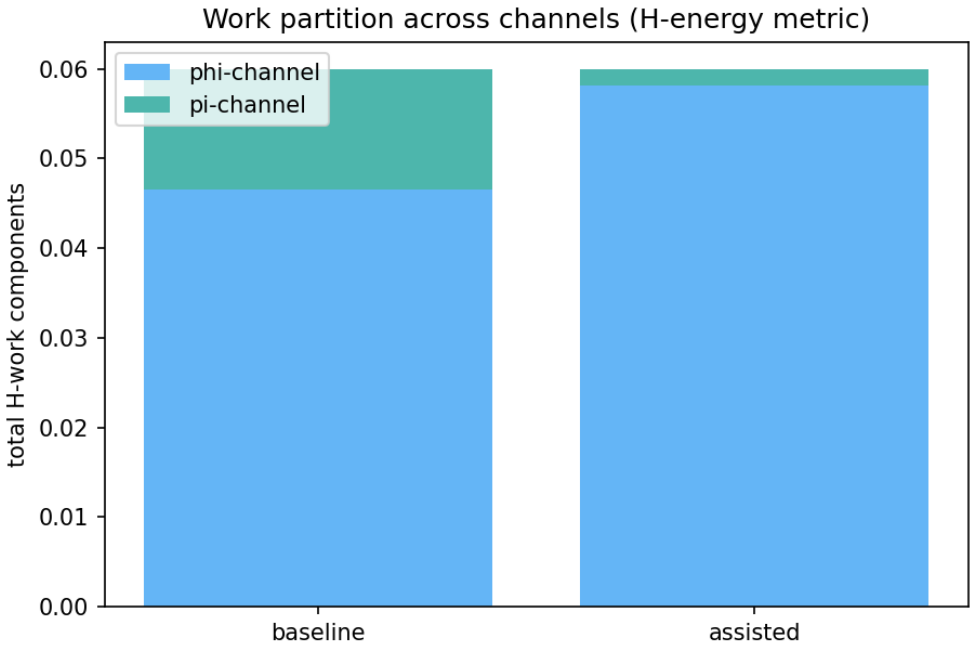

Figure 11: Work partition diagnostics (reverse phase), supporting energy-match (**G3**). Paired artifacts: `logs/20251104_123411_assisted_echo__assisted-echo-t4-prereg-v1c.json`.

References

Google Quantum AI and Collaborators. Observation of constructive interference at the edge of quantum ergodicity. *Nature*, 646:825–830, 2025. doi:10.1038/s41586-025-09526-6. URL `https://doi.org/10.1038/s41586-025-09526-6`.

Google Quantum AI. Supplementary information (moesm1 esm) for s41586-025-09526-6. `https://static-content.springer.com/esm/art%3A10.1038%2Fs41586-025-09526-6/MediaObjects/41586_2025_9526_MOESM1_ESM.pdf`, 2025. Supplementary methods and extended echo diagrams.

X. Li, Y. Zhang, and et al. Quantum computation of molecular geometry via nuclear spin echoes. 2025. URL `https://arxiv.org/abs/2510.19550`.

VDM Project. Void dynamics model canon: Axioms.md. `https://github.com/justinlietz93/Prometheus_VDM/blob/nexus/Derivation/AXIOMS.md`, 2025a. Project axioms and commitments.

VDM Project. Void dynamics model canon: 00_equations.md. `https://github.com/justinlietz93/Prometheus_VDM/blob/nexus/Derivation/z.CANONICAL_Equations/00_EQUATIONS.md`, 2025b. Canonical equations registry.

VDM Project. Void dynamics model canon: Tier_standards.md. `https://github.com/justinlietz93/Prometheus_VDM/blob/nexus/Derivation/TIER_STANDARDS.md`, 2025c. Tier ladder and evidence standards.

Philip J. Morrison. Bracket formulation for irreversible classical fields. *Physica D: Nonlinear Phenomena*, 18 (1-3):410–419, 1986.

Hans Christian Öttinger and Miroslav Grmela. Dynamics and thermodynamics of complex fluids. i. development of a general formalism. *Physical Review E*, 56(6):6620–6632, 1997. doi:10.1103/PhysRevE.56.6620.

Miroslav Grmela and Hans Christian Öttinger. Dynamics and thermodynamics of complex fluids. ii. illustrations of a general formalism. *Physical Review E*, 56(6):6633–6655, 1997. doi:10.1103/PhysRevE.56.6633.

Gilbert Strang. On the construction and comparison of difference schemes. *SIAM Journal on Numerical Analysis*, 5(3):506–517, 1968. doi:10.1137/0705041.

Computations of optimal transport distance with fisher information. `Derivation/References/Reaction-Diffusion/computations-of-optimal-transport-distance-with-fisher-information.pdf`. PDF artifact in repository.

E. L. Hahn. Spin echoes. *Physical Review*, 80:580–594, 1950. doi:10.1103/PhysRev.80.580.

Asher Peres. Stability of quantum motion and fidelity. *Physical Review A*, 30:1610–1615, 1984. doi:10.1103/PhysRevA.30.1610.

R. A. Jalabert and H. M. Pastawski. Environment-independent decoherence rate in classically chaotic systems. *Physical Review Letters*, 86:2490–2493, 2001. doi:10.1103/PhysRevLett.86.2490.

T. Gorin, T. Prosen, T. H. Seligman, and M. Znidaric. Dynamics of loschmidt echoes and fidelity decay. *Physics Reports*, 435(2-5):33–156, 2006. doi:10.1016/j.physrep.2006.09.003.

A. I. Larkin and Y. N. Ovchinnikov. Quasiclassical method in the theory of superconductivity. *Soviet Journal of Experimental and Theoretical Physics*, 28:1200, 1969.

Stephen H. Shenker and Douglas Stanford. Black holes and the butterfly effect. *Journal of High Energy Physics*, 2014(03):067, 2014. doi:10.1007/JHEP03(2014)067.

J. Maldacena, S. H. Shenker, and D. Stanford. A bound on chaos. *Journal of High Energy Physics*, 2016(08): 106, 2016. doi:10.1007/JHEP08(2016)106.

Brian Swingle. Unscrambling the physics of out-of-time-order correlators. *Nature Physics*, 14:988–990, 2018. doi:10.1038/s41567-018-0295-5.

Ernst Hairer, Christian Lubich, and Gerhard Wanner. *Geometric Numerical Integration: Structure-Preserving Algorithms for Ordinary Differential Equations*, volume 31 of *Springer Series in Computational Mathematics*. Springer, 2 edition, 2006. doi:10.1007/3-540-30666-8.

Benedict Leimkuhler and Sebastian Reich. *Simulating Hamiltonian Dynamics*. Cambridge University Press, 2004. doi:10.1017/CBO9780511614118.

Hans Christian Öttinger. *Beyond Equilibrium Thermodynamics*. Wiley, 2005. ISBN 978-0471666585.

Miroslav Grmela. Multiscale thermodynamics. *Entropy*, 20(10):706, 2018. doi:10.3390/e20100706.

Wim van Saarloos. Front propagation into unstable states. *Physics Reports*, 386(2–6):29–222, 2003. doi:10.1016/S0370-1573(02)00538-6.

Justin K. Lietz and Inc. Neuroca. Prometheus_void-dynamics_model. `https://github.com/justinlietz93/Prometheus_VDM`, 2025. Public repository with metriplectic harness, artifacts, and result slugs.

Justin K. Lietz. A logarithmic first integral for the logistic on site law in void dynamics (code + figures + manifests). `https://doi.org/10.5281/zenodo.17220869`, 2025a.

Justin K. Lietz. Echoes of mind: Google's otoc vs vdm's metriplectic echo. PDF artifact within repository, 2025b. GoPenAI article, Oct 2025. PDF available in repository root.

Data-driven reconstruction of a multivariate langevin equation to model complex systems. `Derivation/References/Reaction-Diffusion/data-driven-reconstruction-of-a-multivariate-langevin-equation-to-model-complex-systems.pdf`. PDF artifact in repository.